Supplemental Material for: Heavy carrier effective masses in the van der Waals semiconductor Sn(SeS) revealed by high magnetic fields up to 150 T

Zhuo Yang,[1,*] Xueting Wang,[2] James Felton,[3] Zakhar Kudrynskyi,[3] Masaki Gen,[1] Toshihiro Nomura,[1] Xinjiang Wang,[2] Laurence Eaves,[3] Zakhar D. Kovalyuk,[4] Yoshimitsu Kohama,[1] Lijun Zhang,[2,†] and Amalia Patanè[3,‡]

[1]*Institute for Solid State Physics, The University of Tokyo, Kashiwa, Chiba, 277-8581, Japan*

[2]*Key Laboratory of Automobile Materials of MOE and College of Materials Science and Engineering, Jilin University, 2699 Qianjin Str., 130012, Changchun, China*

[3]*School of Physics and Astronomy, University of Nottingham, Nottingham NG7 2RD, UK*

[4]*Institute for Problems of Materials Science, The National Academy of Sciences of Ukraine, Chernivtsi Branch, Chernivtsi 58001, Ukraine*

(Dated: August 5, 2021)

* zhuo.yang@issp.u-tokyo.ac.jp

† lijun_zhang@jlu.edu.cn

‡ Amalia.Patane@nottingham.ac.uk

I. Estimate of the layer thickness of $SnSe_2$ and SnS_2

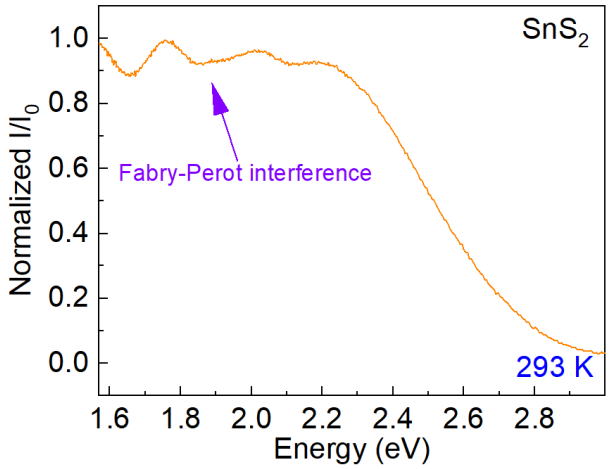

Figure S1. Normalized transmission spectrum measured at T = 293 K for thin films of SnS_2.

Based on the transmission spectrum I/I_0 in FIG. 1(b) and the absorption spectrum of $SnSe_2$ measured by Evans et al.,[1] we estimated the thickness of the $SnSe_2$ film from the Beer-Lambert's law equation[2]

$$I(t) = I_0 e^{-\alpha t}, \tag{S1}$$

where α is the absorption coefficient, t is the film thickness, and I and I_0 are the light intensities transmitted in the presence and absence of the $SnSe_2$ film. When $I/I_0 = 1/e$ is satisfied at a certain photon energy, the absorption coefficient fulfills the condition $\alpha t = 1$. In this way, we estimated the thickness of the $SnSe_2$ film to be $t = 1.4$ μm.

The thickness of SnS_2 film is estimated from the Fabry-Pérot interference fringes observed in the transmission spectra at 293 K (FIG. S1) using[3]

$$t = \frac{hc}{2n\Delta E}, \tag{S2}$$

where h is the Planck constant, c is the speed of light, ΔE is the energy separation between two adjacent peaks, and n is the refractive index. For SnS_2, $n = 3.4$.[4] Using this value, we estimate the thickness of SnS_2 film to be $t = 0.6$ μm.

II. Magneto-transmission of SnS_2 in the Voigt configuration

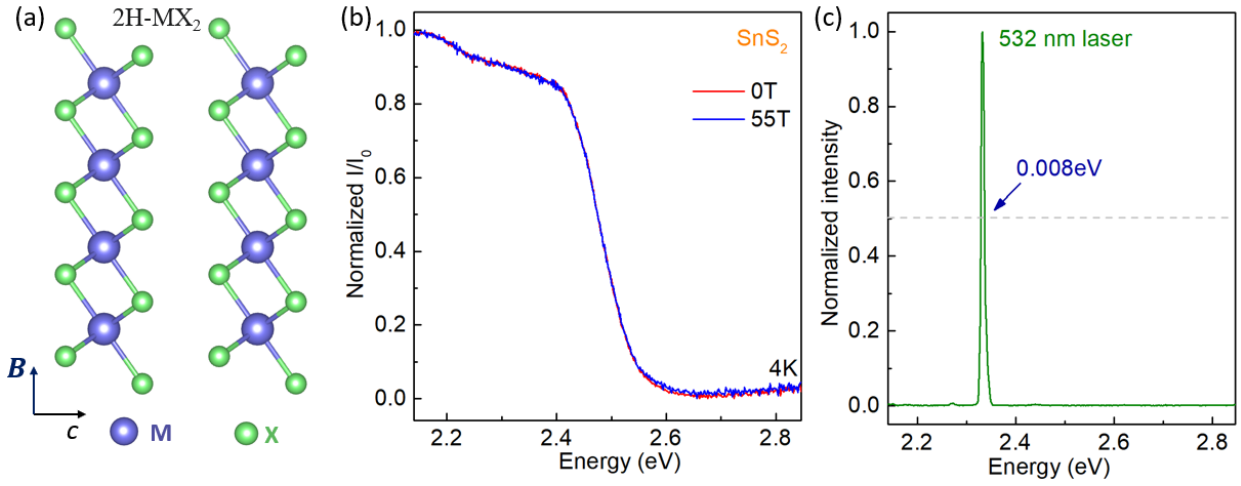

Figure S2. (a) Crystal structure of MX_2 (M = Sn and X = Se, S) and the orientation of magnetic field relative to the a, b and c axis in the Voigt configuration. (b) Magneto-transmission spectra of SnS_2 at 4 K at a given magnetic field. (c) Normalized spectrum of the laser line measured by the spectrometer.

FIG. S2(a) illustrates the crystal structure of MX_2 (M = Sn and X = Se, S) and the orientation of magnetic field relative to the crystal axis in the Voigt configuration (the magnetic field **B** is parallel to the electric field **E** and to the ab layer plane of the crystal). FIG. S2(b) shows the magneto-transmission spectra of SnS_2 at 4 K. The absorption edge of SnS_2 does not show any measurable shift with increasing B up to 55 T. In the Voigt configuration, the cyclotron motion of carriers is parallel to the c axis of the crystal. Thus, the magneto-transmission spectra shown in FIG. S2(b) probe the out-of-plane (z) carrier effective mass. To deduce the low limit value of the out-of-plane reduced electron-hole cyclotron mass μ^*, we estimate the energy resolution in the long pulse field technique by measuring the laser linewidth, as shown in FIG.S2(c). The results indicate that μ^* should be larger than $0.40\,m_e$, consistent with our calculation in Tab. 2.

III. Magneto-transmission of $SnSe_2$ in the Faraday configuration

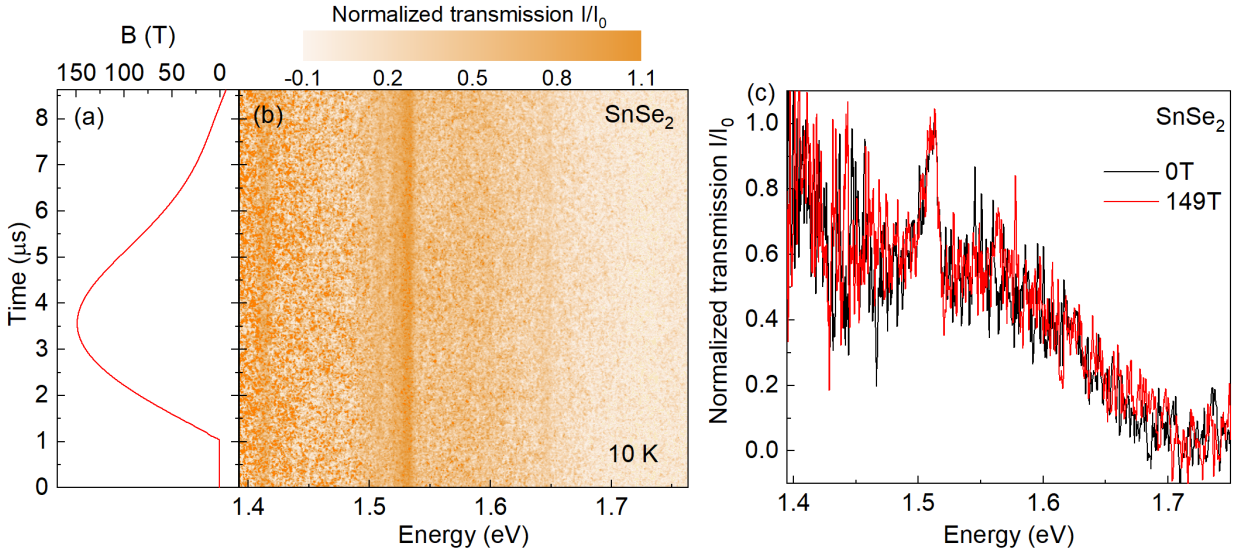

Figure S3. (a) Time dependence of magnetic field B. (b) Streak camera image of the optical transmission of $SnSe_2$ at 10 K with magnetic field of up to $B = 150$ T. (c) Normalized transmission spectra at $B = 0$ T and 150 T.

FIG. S3 shows the magneto-transmission spectra of and $SnSe_2$. FIG. S3(a) shows the time dependence of the magnetic field. The streak camera image is shown in FIG. S3(b). FIG. S3(c) shows a comparison of the zero and maximum field spectra for $SnSe_2$. It can be seen that the absorption edge energy does not depend on the magnetic field B, as also observed for SnS_2 and SnSSe. For $SnSe_2$, the spectra in FIG. S3(c) are noisier than those for $SnSe_{2(1-x)}S_{2x}$ (x = 0.5) and SnS_2. This is due to the low quantum efficiency of the streak camera at low photon energies. We note that the peaks at 1.5 eV in FIG. S3(c) are artificial effects, resulting from the sharp lines of the Xenon lamp spectrum.

IV. Magneto-transmission of InSe

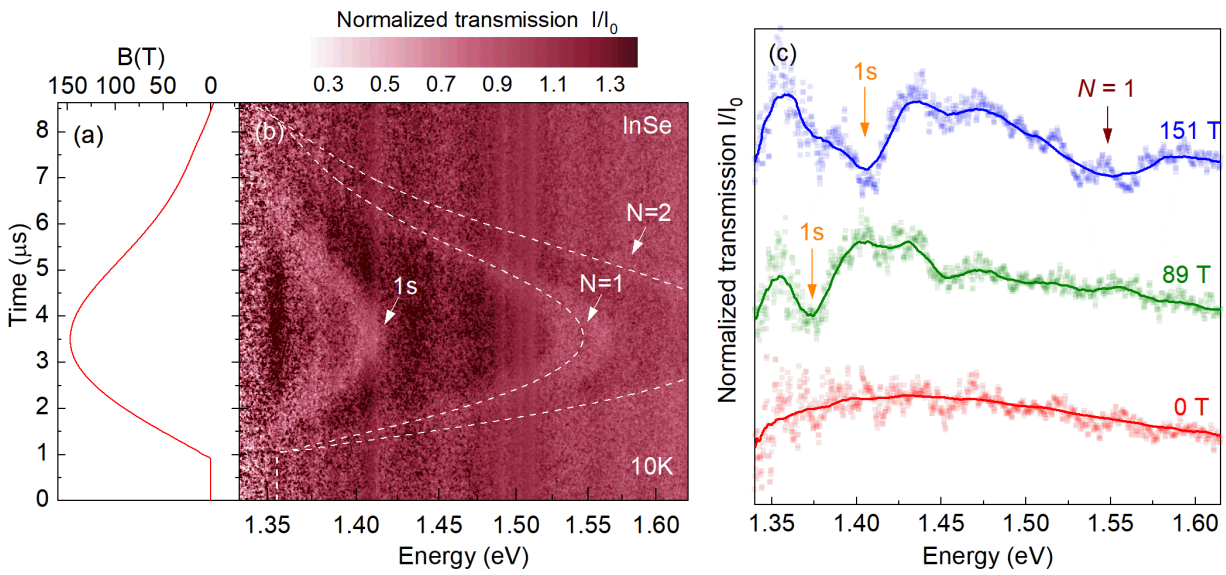

Figure S4. (a) Time dependence of magnetic field B. (b) Streak camera image of the optical transmission for InSe at 10 K with B up to 151 T. White dash lines indicates the fitting for the first ($N = 1$) and second ($N = 2$) Landau level transitions. (c) Normalized transmission spectra at $B = 0$ T, 89 T and 151 T ($T = 10$ K). The spectra are shifted vertically for clarity.

To test the experimental setup, we performed magneto-transmission measurements on thin InSe films using the same setup as for $SnSe_{2(1-x)}S_{2x}$. InSe is a direct band gap semiconductor with well-known electronic properties[5–9]. FIG. S4 shows the magneto-transmission of InSe at magnetic field B of up to 151 T at 10 K. In FIG. S4(b), we can clearly observe three absorption lines, which correspond to the $1s$ excitonic transition and two Landau levels interband transitions ($N = 1, 2$). The white dashed lines indicate the fitting for the Landau levels transitions by the relation $(N + 1/2)\hbar\omega_c^*$ using the reduced electron-hole cyclotron mass μ^* as the only fitting parameter. From the data and analysis, we deduce $\mu^* = 0.138 \pm 0.007\ m_e$, in good agreement with the value in the literature.[5, 8] FIG. S4(c) shows a comparison of the transmission spectra of InSe at a given B. The dot symbols correspond to the measured spectra and are interpolated by solid lines. Due to the responsivity of the streak camera, the absorption edge of InSe at $B = 0$ T is not resolved. However, we can clearly observe the energy shift of the $1s$ excitonic state with increasing B, as well as the Landau quantization at $B = 151$ T. Therefore, we conclude that the weak effect of the magnetic field

on $SnSe_{2(1-x)}S_{2x}$ arises from the large carrier cyclotron masses in this material, rather than a problem with the measurement.

V. Magneto-transmission of SnS_2 with circularly polarized light

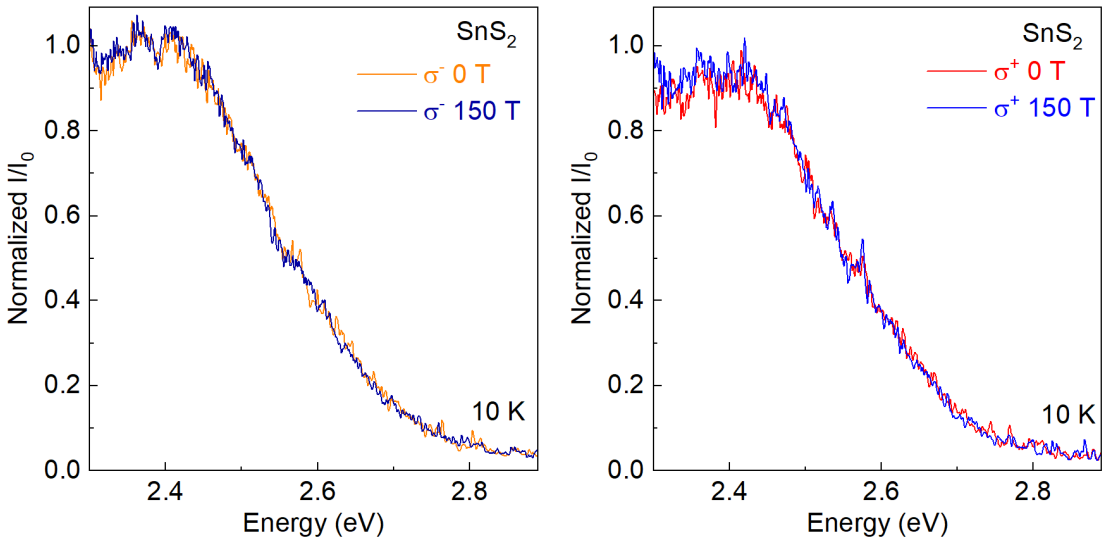

Figure S5. Magneto-transmission spectra of SnS_2 measured at 10 K with magnetic field of up to 150 T. Panel (a) and (b) correspond to left (σ^-) and right (σ^+) circularly polarized light, respectively.

We have conducted magneto-transmission experiments on SnS_2 with circularly polarized light at 10 K and magnetic field of up to 150 T. Circular polarizers were used to generate either left σ^- or right σ^+ circularly polarized light. The result shown in FIG. S5 indicate no Zeeman shift of the transmission. If the cyclotron energy shift is nearly canceled by the simultaneous Zeeman shift, we would expect no energy shift for σ^- ($\hbar\omega_c/2 - g^*\mu_B B/2 \approx 0$), but a significant large energy shift for σ^+ ($\hbar\omega_c/2 + g^*\mu_B B/2$). However, no measurable band edge energy shift was observed for both polarizions. Thus, we exclude this possibility.

VI. Magnetoresistance of $SnSe_2$

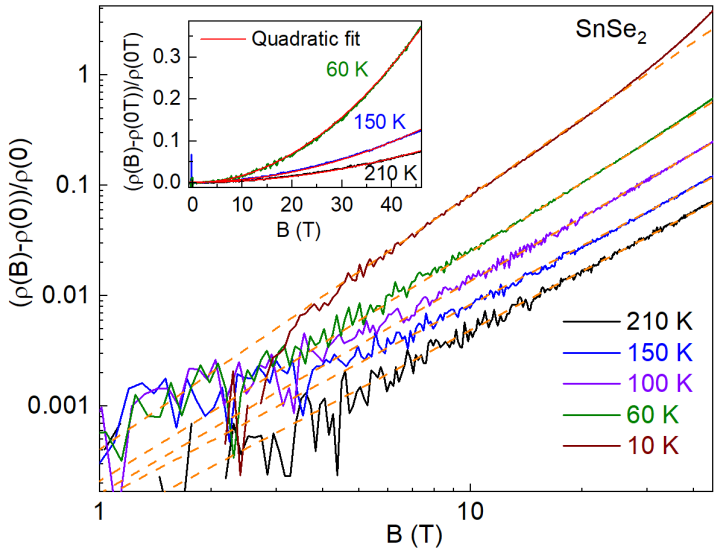

Figure S6. Log-log plot of the magnetoresistance of $SnSe_2$ measured at different temperatures with magnetic field of up to 45 T. Dashed lines are fit to the data by a quadratic magnetoresistance model. Inset: quadratic magnetoresistance of $SnSe_2$.

Magnetoresistance measurements on bulk $SnSe_2$ were performed by a standard four-probe method with the magnetic field applied parallel to the c-axis. FIG. S6 shows a log-log plot of the magnetoresistance ($MR = (\rho(B) - \rho(0))/\rho(0)$) of $SnSe_2$ at different temperatures with magnetic field of up to 45 T. In a higly disordered system, the magnetoresistance tends to show a non-quadratic field dependence.[10, 11] As shown in FIG. S6, the magnetoresistance of $SnSe_2$ depends linearly on the magnetic field in a log-log scale with a slope of 2. In the inset of FIG. S6, we show the quadratic magnetoresistance of $SnSe_2$. Thus, we exclude the possibility that the weak effect of magnetic field on the magneto-transmission of Sn(SeS) is caused by broadening of the Landau levels due to disorder.

VII. Estimate of the energy uncertainty of the measurement equipment at high fields

A. Energy uncertainty from the energy resolution of the measurement equipment

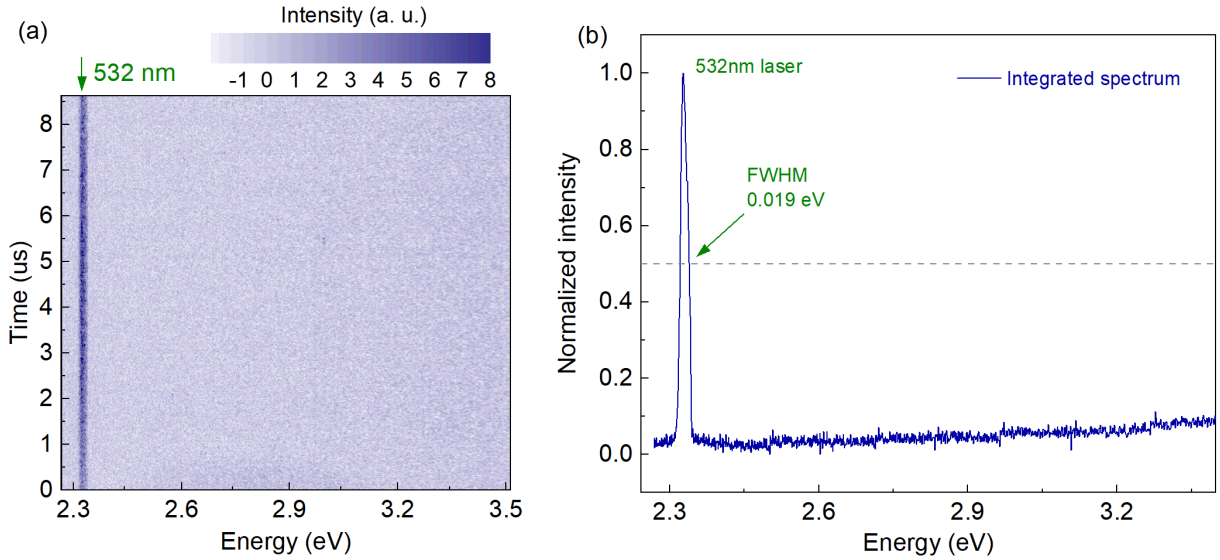

Figure S7. (a) Streak camera image of the laser line. (b) Normalized spectrum of the laser line measured by the streak camera.

We first use the energy resolution of the measurement equipment to constrain the cyclotron mass. To do so, we measured the energy linewidth of an optically pumped semiconductor laser with emission at 532 nm, under the same experimental conditions (same optical path and setting of the streak camera) as used for SnS_2. The product name of the laser is "Sapphire 532 LP" from Coherent Inc. FIG. S7(a) shows the streak image of the laser measured under the same conditions. The extracted laser spectrum from the streak image is shown in FIG. S7(b). The energy resolution of the streak camera is dominated by the instrumental response, which is convoluted with the profile of the laser. The laser linewidth measured by the streak camera is 0.019 eV, broader than the intrinsic laser linewidth. In this case, the measured laser linewidth can be treated as the energy resolution $\Delta E_0 = 0.019\,\mathrm{eV}$. We note that spectroscopy in ultra-high pulse magnetic field is limited by the short acquisition time and optical alignment. Thus, the energy resolution limit in our setup is generally higher than that in zero field spectroscopy techniques.

B. Energy uncertainty from the uncertainty of a fit to the data by a model

We also considered a fit to the transmission data using a theoretical model for the transmission of an indirect band gap semiconductor. We assess the fit uncertainty using an R-squared method to evaluate the scatter of the data points around the fitted line. This is then used to set a constraint on the cyclotron energy.

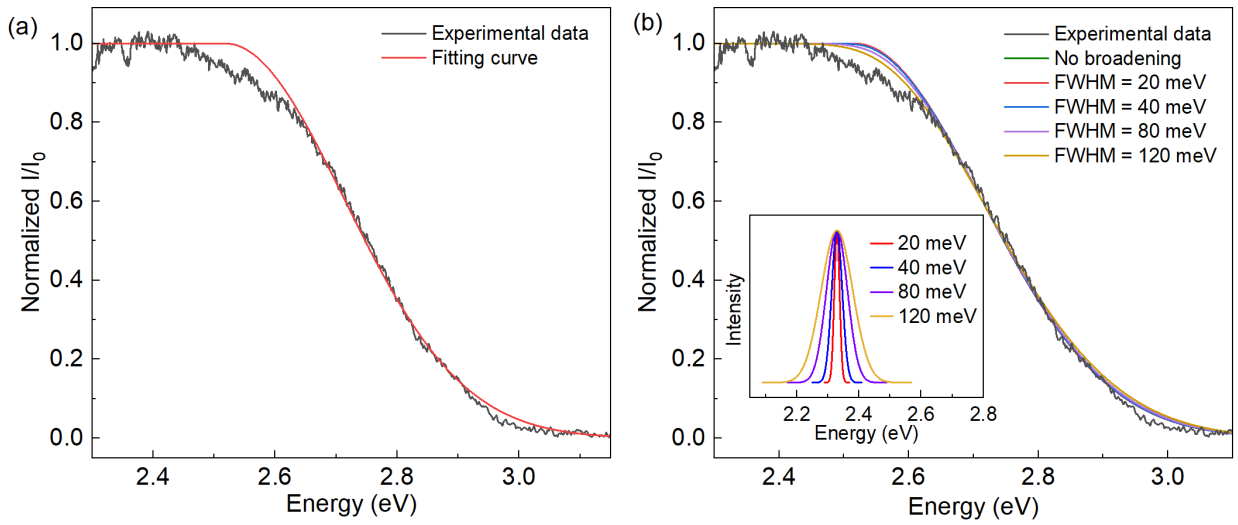

Figure S8. (a) Transmission spectrum of SnS_2 and fitting curve using Eqn. S3. (b) Convolution spectra of an ideal transmission curve with a Gaussion curve of variable linewidth. Inset: Gaussion curves with different linewidth.

An optical transition in an indirect semiconductor is assisted by both phonon-absorption and phonon-emission processes. In our case, the magneto-transmission measurements were performed at low temperature ($T = 10\,\mathrm{K}$). At such low temperature, only phonon emission is involved in the optical transitions [3]. The ideal absorption spectrum of an indirect band gap semiconductor with phonon emission is described by [3],

$$\alpha = A\frac{(\hbar\omega - E_g - \hbar\omega_0)^2}{1 - e^{-\hbar\omega_0/k_BT}}, \tag{S3}$$

where α is the absorption coefficient, $\hbar\omega$ and $\hbar\omega_0$ are the photon and phonon energy, respectively, k_B is the Boltzmann constant, E_g is the indirect band gap energy and A is a constant. The phonon energy $\hbar\omega_0$ of SnS_2 is set at $32.2\,\mathrm{meV}$ [12]. We use Eqn. 3 to fit the transmission spectra, as shown in FIG. S8 (a). The fitting to the transmission data is overall good except for the discrepancy in the onset energy region of the absorption. This discrepancy

may result from the broadening of the transmission due to the laser line and/or disorder. Thus, we considered the convolution of the ideal transmission curve with a Gaussian curve, as shown in FIG. S8 (b).

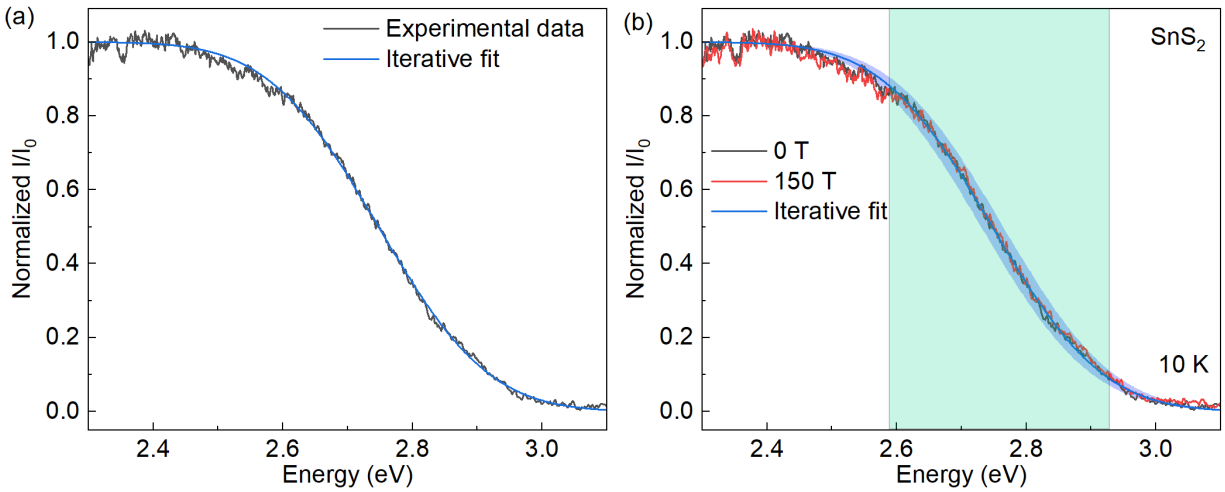

Figure S9. (a) Transmission spectrum of SnS_2 and its iterative model fitting. (b) Transmission spectrum of SnS_2 at 0 T and 150 T and iterative model fitting with variable band gap energy.

An iterative method based on the model mentioned above was used to fit the transmission spectra, as shown in FIG. S9 (a). Based on this model, the band gap energy of SnS_2 is estimated to be $E_g = 2.690$ eV at $B = 0$ T and $E_g = 2.688$ eV at $B = 150$ T. The difference between these two values is within the uncertainty in the value of E_g. To estimate the uncertainty in the value of E_g, its value was varied about the best fit until 95% (2σ) of the data in the highlighted regions was encompassed (see FIG. S9 (b)). This gave the following value for the uncertainty: 2σ =17 meV. Thus, the energy uncertainty value estimated from the fitting uncertainty is very close to that from the laser linewidth. Based on this theoretical model, we determined a lower limit for the cyclotron mass of 0.511 m_e.

In summary, the energy uncertainties deduced from these two models are quite similar, and yield a similar lower limit value for the cyclotron mass. There is no doubt that it would have been preferable to measure a shift to assess the mass. However, even our most conservative estimate of the lower limit of the cyclotron mass is heavier than that of most well-known semiconductors. This is the main finding of the manuscript.

VIII. Conductivity effective masses

Table S1. Conductivity effective masses for electrons (m_e^*), holes (m_h^*) in SnS_2 and $SnSe_2$, as calculated using the semiclassical Boltzmann transport theory at 300 K. The Cartesian directions are x along a, y along b, and z normal to x and y (c-axis).

		Carrier concentration	m_t^*/m_e		m_l^*/m_e	
Compound		(cm^{-3})	x	y	z	$\overline{m}^*/m_e$
SnS_2	m_h^*/m_e	10^{15}	4.124	4.124	0.481	1.169
		10^{16}	4.091	4.091	0.447	1.161
		10^{18}	4.082	4.082	0.476	1.158
	m_e^*/m_e	10^{15}	0.447	0.447	1.117	0.559
		10^{18}	0.442	0.442	1.105	0.552
		10^{20}	0.519	0.519	2.167	0.702
$SnSe_2$	m_h^*/m_e	10^{15}	1.101	1.101	0.649	0.893
		10^{16}	1.205	1.205	0.711	0.978
		10^{18}	1.208	1.208	0.713	0.981
	m_e^*/m_e	10^{15}	0.392	0.392	0.689	0.458
		10^{18}	0.354	0.354	0.623	0.414
		10^{20}	0.396	0.396	0.472	0.493

We use Boltzmann transport calculations applied to the calculated band structures to extract the conductivity effective mass for electron and hole motion along different crystallographic directions, in the layer plane (m_t^*) and out-of-plane (m_l^*), and their geometric average $\overline{m}^*$. In this model, we consider a range of carrier concentrations for electrons and holes. Tab. S1 shows the calculated conductivity effective mass for electrons and holes in SnS_2 and $SnSe_2$ with different carrier concentrations. It can be seen that the masses change by less than 10 % with increasing carrier concentration up to $10^{18}\,cm^{-3}$.

[1] B. Evans and R. Hazelwood, Optical and electrical properties of $SnSe_2$, J. Phys. D Appl. Phys. **2**, 1507 (1969).

[2] N. Peyghambarian, S. W. Koch, and A. Mysyrowicz, *Introduction to semiconductor optics* (Prentice-Hall, Inc., 1993).

[3] A. Lipson, S. G. Lipson, and H. Lipson, *Optical physics* (Cambridge University Press, 2010).

[4] E. Rusu, N. Syrbu, A. Tiron, and V. Zalamai, Band structure and optical constants of SnS_2 single crystals, Mater. Res. Express **6**, 046203 (2019).

[5] E. Kress-Rogers, R. J. Nicholas, J. C. Portal, and A. Chevy, Cyclotron resonance studies on bulk and two-dimensional conduction electrons in InSe, Solid State Commun. **44**, 379 (1982).

[6] J. Camassel, P. Merle, H. Mathieu, and A. Chevy, Excitonic absorption edge of indium selenide, Phys. Rev. B **17**, 4718 (1978).

[7] M. Millot, S. Gilliland, J. M. Broto, J. Gonzalez, J. Leotin, A. Chevy, and A. Segura, High pressure and high magnetic field behaviour of free and donor-bound-exciton photoluminescence in InSe, Phys. Status Solidi B **246**, 532 (2009).

[8] M. Millot, J.-M. Broto, S. George, J. González, and A. Segura, Electronic structure of indium selenide probed by magnetoabsorption spectroscopy under high pressure, Phys. Rev. B **81**, 205211 (2010).

[9] G. W. Mudd, M. R. Molas, X. Chen, V. Zólyomi, K. Nogajewski, Z. R. Kudrynskyi, Z. D. Kovalyuk, G. Yusa, O. Makarovsky, L. Eaves, M. Potemski, V. I. Fal'ko, and A. Patanè, The direct-to-indirect band gap crossover in two-dimensional van der Waals Indium Selenide crystals, Sci. Rep. **6**, 39619 (2016).

[10] M. Parish and P. Littlewood, Non-saturating magnetoresistance in heavily disordered semiconductors, Nature **426**, 162 (2003).

[11] N. Kozlova, N. Mori, O. Makarovsky, L. Eaves, Q. Zhuang, A. Krier, and A. Patanè, Linear magnetoresistance due to multiple-electron scattering by low-mobility islands in an inhomogeneous conductor, Nat. Commun. **3**, 1 (2012).

[12] Z. R. Kudrynskyi, X. Wang, J. Sutcliffe, M. A. Bhuiyan, Y. Fu, Z. Yang, O. Makarovsky, L. Eaves, A. Solomon, V. T. Maslyuk, Z. D. Kovalyuk, L. Zhang, and A. Patanè, Van der Waals $SnSe_{2(1-x)}S_{2x}$ Alloys: Composition-Dependent Bowing Coefficient and Electron–Phonon In-

teraction, Adv. Funct. Mater. **30**, 1908092 (2020).